Direct imaging of cross-sectional magnetization reversal in an exchange-biased CoFeB/IrMn bilayer

Shuai Hu,[1,2,3] Ke Pei,[1,2,4] Baomin Wang,[1,2,*] Weixing Xia,[1,2,†] Huali Yang,[1,2] Qingfeng Zhan,[1,2] Xiaoguang Li,[5,6] Xincai Liu,[4] and Run-Wei Li[1,2,‡]

[1]*CAS Key Laboratory of Magnetic Materials and Devices, Ningbo Institute of Materials Technology and Engineering, Chinese Academy of Sciences, Ningbo 315201, People's Republic of China*

[2]*Key Laboratory of Magnetic Materials and Application Technology, Ningbo Institute of Materials Technology and Engineering, Chinese Academy of Sciences, Ningbo 315201, People's Republic of China*

[3]*Nano Science and Technology Institute, University of Science and Technology of China, Suzhou 215123, People's Republic of China*

[4]*Faculty of Materials Science and Chemical Engineering, Ningbo University, Ningbo 315211, People's Republic of China*

[5]*Hefei National Laboratory for Physical Sciences at Microscale and Department of Physics, University of Science and Technology of China, Hefei 230026, People's Republic of China*

[6]*Collaborative Innovation Center of Advanced Microstructures, Nanjing 210093, People's Republic of China*

(Received 22 February 2017; revised manuscript received 25 December 2017; published 21 February 2018)

The exchange coupling between ferromagnetic (FM) and antiferromagnetic materials has been intensely studied for fundamental physics and technological applications in various devices. However, the experimental reported magnitudes of exchange coupling are often smaller than that predicted theoretically, and for which the formation of springlike spin structure in the FM layer has been suggested as the cause. However, investigating the spin structure around the interface of exchange-coupled systems is challenging. Here we report the direct imaging of the cross-sectional magnetization reversal and spin structure at the interface of a model exchange-biased CoFeB/IrMn bilayer by a Lorentz transmission electron microscope with electron holography techniques. Through imaging of *in situ* magnetization reversal and spin structure at the remanent state, the springlike spin structure (either Bloch-wall-like or Néel-wall-like) in the CoFeB layer has been deduced within subnanometer region of the interface. This result puts a strong constraint on the theories of exchange coupling in inhomogeneous magnetic systems.

DOI: 10.1103/PhysRevB.97.054422

I. INTRODUCTION

Exchange bias (EB) produces a shift of the hysteresis loop of a ferromagnetic (FM) material along the magnetic-field axis due to the coupling with an adjacent antiferromagnetic (AFM) material [1,2]. The magnitude of this shift is defined as the exchange-bias field (H_{EB}). This effect has been widely employed for various important applications [2–6], one of which is spin-valve devices. In such devices, the FM layer adjacent to an AFM layer has its magnetic state stabilized and allows magnetoresistance to be developed in a small field [3].

Since the magnetic interaction between AFM and FM layers are short-ranged while FM domain walls evolve with a relatively long scale, the EB phenomenon was originally assumed to be an interfacial effect [7]. However, recent experiments [8–10] and theories [11] have shown that EB is affected by long-range interactions in the AFM or FM layer. The spin structure in the bulk of the AFM or FM layer appears to be crucial for the magnitude of H_{EB}, which is always a two-to-three orders smaller than theoretically predicted value [7]. The FM spin structure induced by breaking of the time-reversal symmetry results in an asymmetric magnetization reversal, which has been suggested by experiments from polarized neutron reflectometry [12], photoemission electron microscopy [13], magnetotransport [14], and the magneto-optical Kerr effect [15]. More recently, Morales *et al.* proposed that springlike FM domain walls, which are parallel to the AFM/FM interface, exist in EB systems [10]. The relevant micromagnetic simulation results also supported a hybrid interfacial domain wall extending into AFM and FM layers [16,17]. The spring spin structure caused by opposite pinning directions in AFM/FM/AFM trilayers can be distributed through the total 50-nm FM layer [17], suggesting that the detection of depth-dependent magnetic profiles or spin structure of FM layer in EB systems is not trivial. However, investigating the magnetization reversal process in the cross-sectional thin films is challenging, due to the resolution and depth limitations of conventional microscopy techniques.

Electron holography combined with Lorentz transmission electron microscopy (L-TEM) is a powerful tool for characterizing the magnetic and electrical-field distribution in materials. It has been used to investigate the micromagnetic domain structure in nanoparticles, nanowires, and skyrmion lattices for its high spatial resolution [18–23]. $Co_{40}Fe_{40}B_{20}$ (CoFeB)/$Ir_{20}Mn_{80}$ (IrMn) is a model exchange-bias system, which has been widely used in spintronic devices [24–26]. In this work, we directly visualized the cross-sectional magnetic structure of the FM layer in exchange-biased CoFeB/IrMn bilayer and its evolution under magnetic field by high-resolution

*wangbaomin@nimte.ac.cn
†xiawxing@nimte.ac.cn
‡runweili@nimte.ac.cn

electron holography in L-TEM. Within the spatial resolution of our L-TEM (∼2.3 nm), neither Bloch-wall-like nor Néel-wall-like spin structure has been observed near the interface. This result indicates that the magnitude of H_{EB} may be determined by subnanometer springlike spin structure in exchange-biased CoFeB layer at the interface. Therefore, theoretical modeling of exchange bias should take this into consideration to design a new structure with large H_{EB} and coercivity. Our results are also of great relevance for designing rare-earth-free permanent composite magnets comprising two phases.

II. EXPERIMENT

Ta (2 nm)/CoFeB (t_{FM})/IrMn (30 nm)/Ta (2 nm) stacks were deposited on Si substrates. The samples were grown by magnetron sputtering in an Ar atmosphere of 2.0×10^{-3} mTorr with a base pressure of $<5 \times 10^{-8}$ Torr at room temperature. 2-nm-thickness tantalum was used to protect the CoFeB from oxidation. During deposition, a small magnet field was applied to make sure the FM layer remains at saturated state. The magnetic properties were measured using the magneto-optical Kerr effect (MOKE). Phase images of both Bloch-wall-like and Néel-wall-like spin structure were simulated by calculating the phase images based on the relations between vector potential and magnetic dipole, the phase shift, and vector potential.

The samples for L-TEM study were fabricated using focused ion beam (FIB) and scanning electron microscope dual-beam system (Zeiss Auriga) combined with a gas injection system and micromanipulator (Omniprobe 200+, Oxford). Two coating layers were deposited as the protecting layers at the surface of sample. After general FIB milling process, the coating layers above the L-TEM sample were removed by the FIB probe to make the observation area connected directly with the vacuum, which is important to get the ideal signals for electron holography observation. For the high-resolution electron holography study, the thickness of sample is about 80 nm.

Our L-TEM is a specially designed JEM-2100F TEM with a dedicated object lens for observing the magnetic domain structure. The specimen is inserted into the upper polepiece. The stray field at the position of specimen is approximately 4 Oe. Due to a large stray field of 350 Oe at the entrance of the specimen holder, the object lens is always turned off when the holder is to be inserted or pulled out to avoid the influence of the stray field. Although the lattice resolution is degraded by the special object lens, it can still reach 0.45 nm. An electron biprism is installed in our TEM to carry out the electron holography experiment. We have a magnetic-field holder to apply variable fields from −600 to 600 Oe in the plane of specimen *in situ*.

III. RESULTS AND DISCUSSION

A. Microstructures and exchange-bias effect

Figure 1(a) gives an overview of the film; clear CoFeB/IrMn interfaces between different layers are observed. Selected area electron diffraction (SAED) of CoFeB was conducted over the region indicated by the circle, which reveals an amorphous structure of CoFeB. It is worth mentioning that amorphous structure is beneficial for electron holography

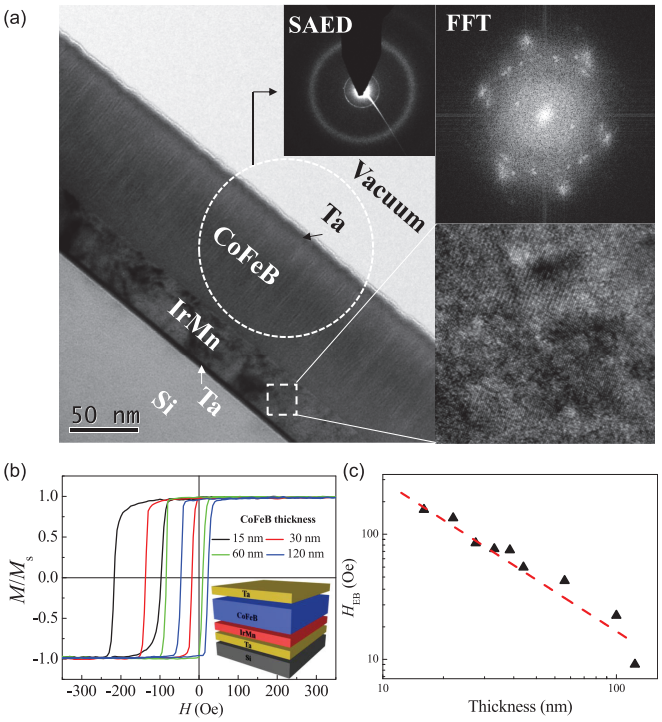

FIG. 1. (a) The microstructure images of CoFeB/IrMn stack. The insets on the right are SAED of CoFeB and FFT image of IrMn, respectively (the white circle area is selected for SAED and the square area for high-resolution TEM and FFT). (b) Hysteresis loop of IrMn/CoFeB exchange-bias bilayers measured by MOKE for different FM thickness. The inset shows the stack of the sample. (c) FM thickness dependence of the H_{EB}, which performs a reciprocal relation ($1/t_{FM}$ dependence of H_{EB}).

because it rules out the electron scattering from crystalline lattice. The IrMn is polycrystalline, which can be seen from the high-resolution TEM image (the bottom-right corner) and its corresponding fast Fourier transformation (FFT) (the top-right corner). Figure 1(b) shows hysteresis loops of samples with different CoFeB thickness (t_{FM}) of 15, 30, 60, and 120 nm, respectively. All the H_{EB} values are roughly around hundreds of oersted, which is consistent with previous reports of Fe-based exchange-bias system [27]. Furthermore, the FM thickness dependence of the H_{EB} in a logarithmic scale is shown in Fig. 1(c), which reveals a $1/t_{FM}$ dependence of H_{EB}.

B. Electron holography

Off-axis electron holography is a powerful technique to detect the phase shift of electron wave caused by magnetic- and electric fields in its traveling path. The electric fields are related to mean inner potential and specimen thickness [28]. Figure 2 shows the electron holography image and data processing of IrMn/CoFeB specimen, which is prepared with the exchange-bias direction parallel to the specimen plane. Figure 2(a) is the electron hologram of the cross section of exchange-biased CoFeB/IrMn multilayers. Figure 2(b) is the phase image of the electron wave, which is obtained from Fig. 2(a) through the digital reconstruction process with the HOLO WORKS software package. Along the yellow line (*AB*)

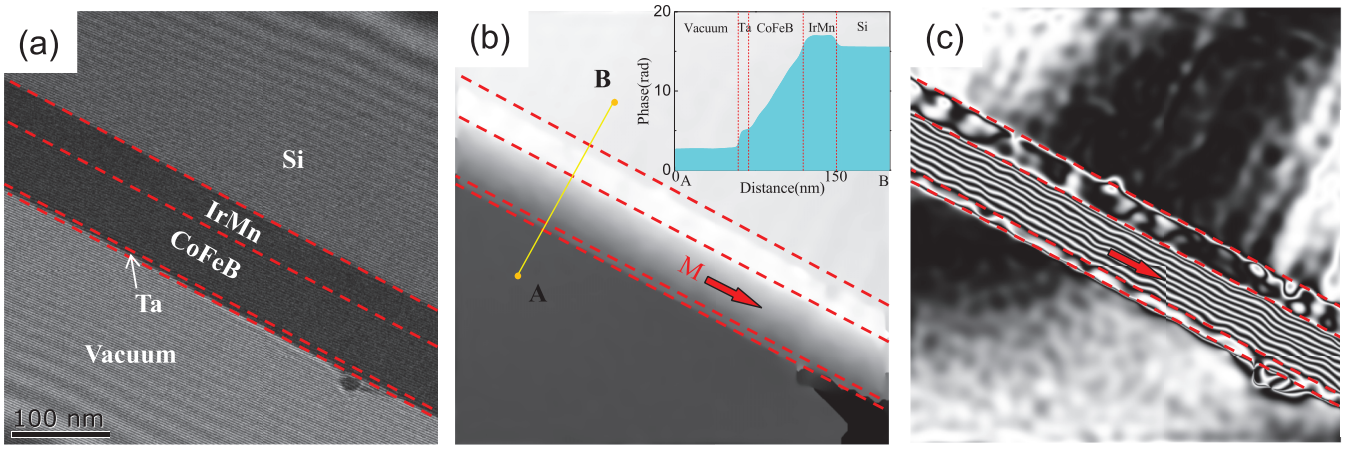

FIG. 2. (a) Electron hologram of cross-sectional IrMn/CoFeB multilayers. (b) The unwrapped phase image and the inside image show the phase profile from position A to position B, which is the positive gradient direction of electron wave phase in CoFeB layer. (c) The reconstructed phase image displayed in cosine function with phase amplification of 5.

shown in the inset of Fig. 2(b), the phase gradients of vacuum area, Ta layer, IrMn layer, and Si substrate are almost zero, indicating the thickness of the TEM sample is uniform. The phase gradient in the CoFeB layer in Fig. 2(b) depends on the direction of magnetization in the specimen. By applying the right-hand rule, the direction of magnetic field can be determined, i.e., extend the right hand with thumb pointing to the opposite direction of traveling electron; make the palm direction the same as deflection of the electron which is the increasing direction of phase; then the four fingers point to the direction of the magnetic field [29]. For example, phase increasing in the CoFeB layer along the direction of A to B shown in the inset of Fig. 2(b) suggests that the magnetization points in the direction indicated by the red arrow. The phase can be displayed more clearly in cosine function with phase amplification of 5 as shown in Fig. 2(c). The density and tangent direction of black (or white) lines in Fig. 2(c) represent the strength and direction of magnetic flux density, respectively, which is the integration of the projected component on the specimen plane along specimen thickness in incident beam direction. The magnetization is considered to be equal to magnetic flux density, because the demagnetized field can be ignored in the longitudinal direction. It is shown that the magnetization of the CoFeB layer is parallel to film plane and no magnetic signals exist in the vacuum area, Ta layer, IrMn layer, and Si substrate.

C. Simulations of the phase images of Bloch-wall-like and Néel-wall-like walls at the interface

Whether the magnetization switching is coherent or incoherent is difficult to capture due to the extremely short time of the process. On the other hand, with external field being applied, the static magnetic state determined by Zeeman energy and exchange energy might reveal nonuniform magnetization distribution, e.g., some forms of domain walls in the CoFeB layer. Here, we firstly calculated the phase images of Bloch-wall-like and Néel-wall-like spin structures at the interface.

According to the classical electromagnetism, the vector potential $\vec{A}$ of a magnetic dipole $\vec{m}$ can be expressed by

$$\vec{A} = \frac{\mu_0}{4\pi}\frac{\vec{m}\times\vec{R^0}}{R^2}. \tag{1}$$

$\vec{A}$ is the vector potential at point P produced by a magnetic dipole $\vec{m}$ located at origin O; $\vec{R^0}$ and R are the direction vector of $\overrightarrow{OP}$ and the length of OP, respectively [Fig. 3(a)]. If spin (dipole) texture such as Bloch-wall-like or Néel-wall-like is given [Figs. 3(b) and 3(c), in the xy plane of Fig. 3(a)], the vector potential $\vec{A}$ at an arbitrary point in space can be obtained by calculating $\vec{A}$ produced by the single dipoles and summing them up. On the other hand, the phase shift φ of electron beam is expressed by

$$\varphi = \frac{e}{\hbar v}\int V ds - \frac{e}{\hbar}\int \vec{A}d\vec{s}, \tag{2}$$

where e, $\hbar$, v, and V are electron charge, Planck's constant divided by 2π, electron velocity, and electrical potential, respectively. The first term in the right side of Eq. (2) is the phase shift caused by electric potential and the second term is that caused by magnetic potential. Here we do not consider the influence of electric potential. If the component of vector potential projected to the electron-beam direction is integrated along the electro-beam path [z direction in Fig. 3(a)], the phase shift of electron beam caused by magnetic potential can be obtained. In the calculations, Block-wall-like and Néel-wall-like spin structures are shown in Figs. 3(b) and 3(c), respectively. The phases in the red blocks are taken and shown in order to simulate the experiment where only a part of the specimen can be observed. Figures 3(d) and 3(e), and 3(f) and 3(g) show the phase images in direct phase value and in cosine function, respectively, for Bloch-wall-like/Néel-wall-like spin structures. We can see that quite different images could be observed for the two different kinds of spin structures. The density of phase contour lines would become lower where the in-plane magnetization component becomes lower for a Bloch-wall-like reversal type [Fig. 3(f)], while the direction of magnetization

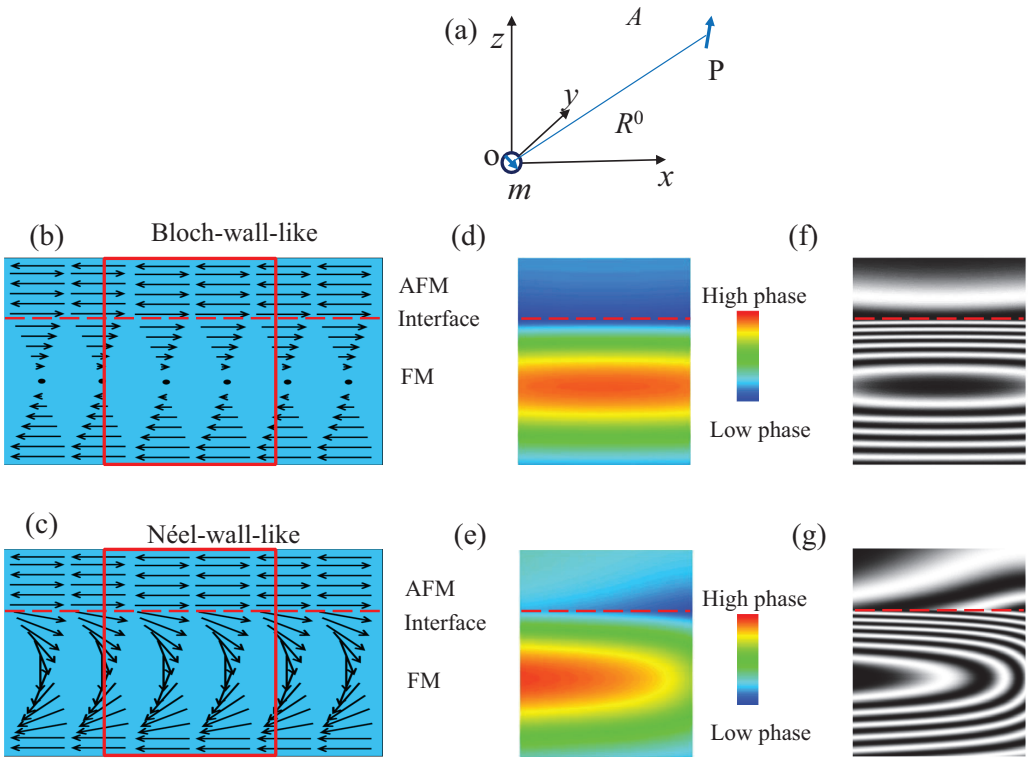

FIG. 3. (a) The vector potential of a magnetic dipole in Cartesian coordinate system. (b), (c) Schematics of Bloch-wall-like and Néel-wall-like spin structures, respectively. (d), (e) Calculated phase images of Bloch-wall-like and Néel-wall-like spin structures, respectively. (f), (g) Phase images indicated by cosine function of Bloch-wall-like structure and Néel -wall-like spin structures, respectively.

change by Néel-wall-like reversal type would cause the straight contour lines to become continuous ellipses [Fig. 3(g)].

D. *In situ* observation of magnetization reversal

In order to explore the magnetization reversal process in details, an *in situ* experiment was carried out with magnetic field applied to the specimen with t_{FM} of 120 nm. In this condition, the TEM magnification is 40 k in low magnification (LOWMAG) mode and the biprism voltage is 120 V. A series of phase images with field steps of 10 Oe were obtained and some of them are shown in Fig. 4(a). When a field of −450 Oe is applied, uniform contour lines are obtained in the CoFeB layer and the magnetization points downward, which is determined by the gradient of phase distribution. When a field between −200 and +440 Oe is applied, no changes of magnetization in direction and strength are observed. However, when the field is increased to +450 Oe, an abrupt complete magnetization reversal in the whole CoFeB layer occurs; when the field is further increased to +460 and +500 Oe, no distinct changes in phase images of the CoFeB layer are observed. Opposite experiments with fields decreasing from +600 to −600 Oe were also carried out and magnetization reversal occurred at −460 Oe. Note that the phase shifts of the two different magnetic states are not the same, which is caused by electric potential contribution from the CoFeB layer. Phase images of one state (①–③) are the sum of magnetic and electric potentials, and of another state (④–⑥) are the difference of them. Based on the strength and direction of magnetization estimated from the phase images (not all of them are shown), the hysteresis loop is depicted in Fig. 4(b). From the *in situ* experiments, we find that although the H_{EB} remains the same, the coercivity of TEM specimens is always much higher than that of the large-area thin films, which may be caused by the large shape anisotropy of the TEM specimen. The *in situ* magnetization reversal measurements show that the magnetization of CoFeB is uniformly distributed across the FM layer; no Bloch-wall-like or Néel-wall-like spin structure like those in Figs. 3(f) and 3(g) is observed in this dynamic process. This is also more clearly confirmed by the almost constant derivatives of phase line profiles along yellow lines [Fig. 4(c)].

However, we cannot reach a high resolution in the *in situ* experiments because it has to be carried out in LOWMAG mode with object lens off in our Lorentz microscope. Due to a large electromagnet in the holder, if the object lens is switched on when the holder is being inserted, the interaction between the electromagnet of the holder and polepiece of the object lens becomes complicated, leading to an unknown electron path and uncertain field acting on the specimen. Under this LOWMAG mode, the maximum magnification is only 40 k and hence the resolution of holography is restricted, which is about 15.6 nm (interference fringe spacing: 5.22 nm, fringe contrast: 25.2%) with overlap width of 585 nm. On the other hand, in MAG mode with object lens on the resolution of electron holography in our L-TEM can reach about 2.3 nm (interference fringe spacing: 0.77 nm, fringe contrast: 27.5%) with overlap width of 155 nm, but it can only work in zero applied field with an

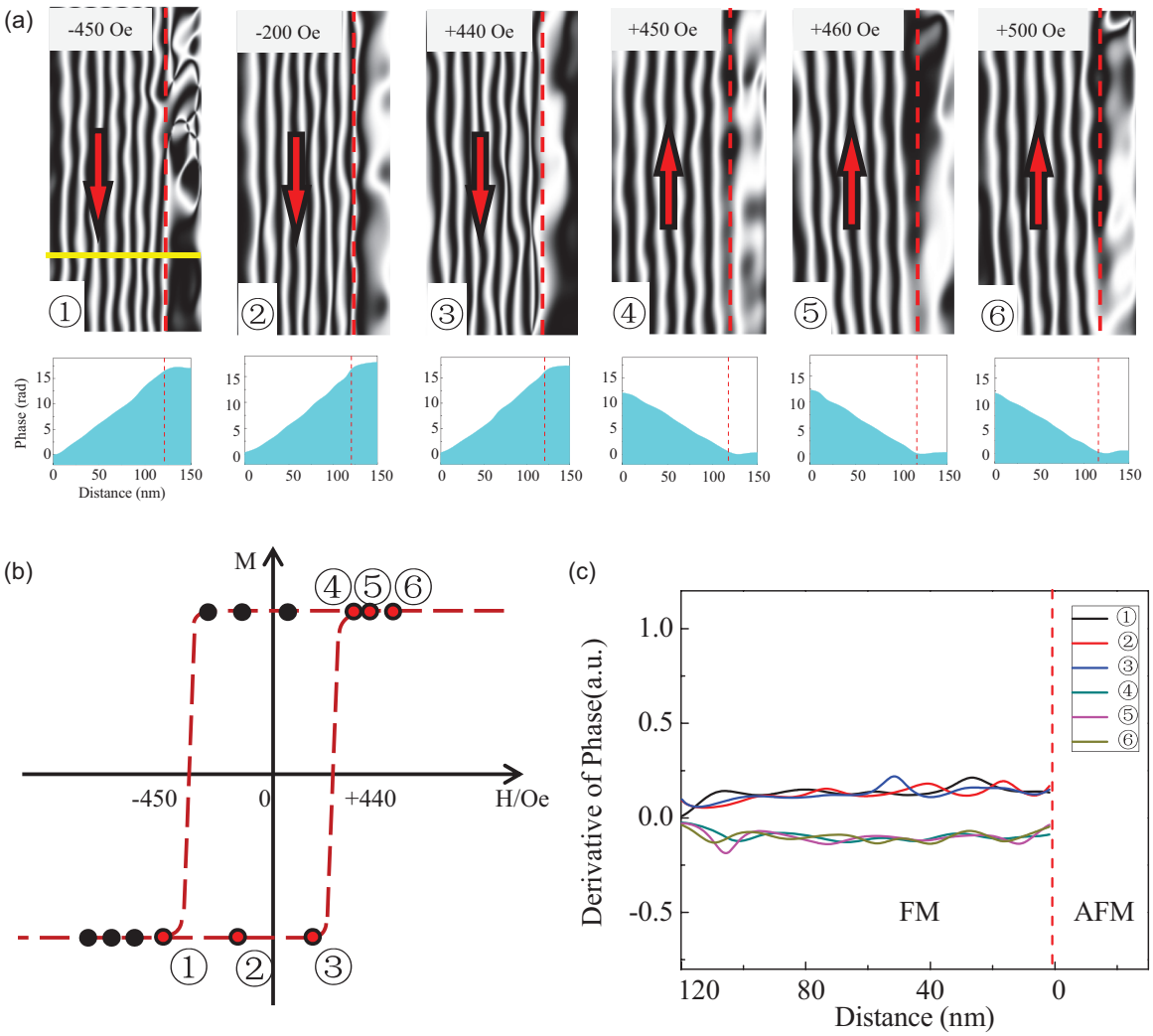

FIG. 4. (a) Selected reconstructed phase images (displaying in cosine function with phase amplification of 5) under different applied magnetic fields, and the corresponding phase profiles. (b) The hysteresis loop is obtained by the *in situ* magnetic-field phase images. (c) Derivative of phase with respect to position in ①–⑥.

ordinary specimen holder. That is, only the remanent state at the FM/AFM interface can be imaged. For the CoFeB/IrMn samples, it is found from both hysteresis loops and *in situ* observations that two remanent states exist for 60- and 120-nm CoFeB layer samples [Fig. 1(b)].

Furthermore, in MAG mode, a two-side-subtraction method can be adopted to remove the influence of inner potential, which offers an exact image of magnetization distribution. As shown in Eq. (2), the contributions of electric potential and magnetic potential have opposite signs; if we take phase images with electron beam incident from one side and the other by turning over the specimen, the subtraction of two phase images can remove the contribution of electric potential, which is a valuable method of evaluating magnetic information in electron holography experiments [30]. Following this method, we obtain the results in Figs. 5(a) and 5(b) that the magnetization is uniformly distributed and the specimen thickness is uniform across the CoFeB layer. In the next section, we will focus on the interface between CoFeB and IrMn layers to investigate the spin structure in the high-resolution mode.

E. Observation of magnetization distribution at the remanent state in the high-resolution mode

The magnetization of CoFeB is parallel to the exchange-bias direction at the remanent state *A* (decreasing the field from

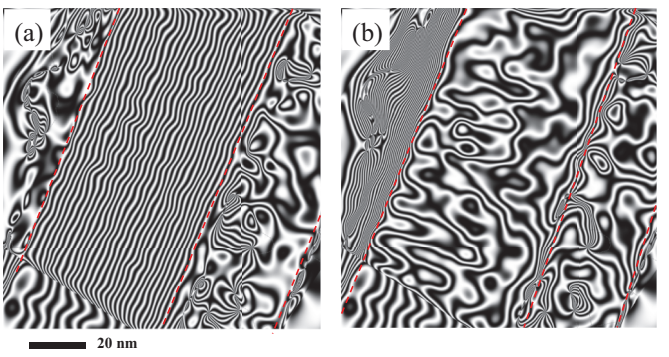

FIG. 5. (a), (b) Phase images of magnetic information and electrical information through all CoFeB layer obtained by two-side-subtraction method, respectively.

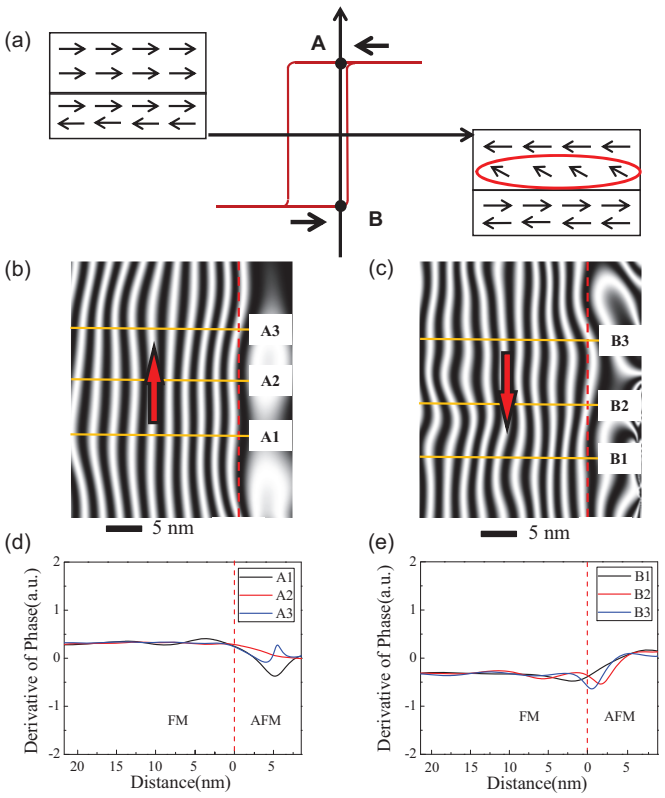

FIG. 6. (a) Schematic configuration of magnetization at remanent points A and B. (b), (c) Phase images at A and B in (a), which only show the details near the interface, respectively. The contribution of inner potential has been removed. (d), (e) Phase derivatives with respect to distance to CoFeB/IrMn interface along $A1$, $A2$, and $A3$ in (b) and $B1$, $B2$, and $B3$ in (c).

positive saturation field to zero) and antiparallel at the remanent state B (increasing the field from negative saturation field to zero field) as shown in Fig. 6(a). In this condition, the TEM magnification is 180 k in MAG mode and the biprism voltage is 130 V. In remanent state A, the magnetization direction of CoFeB is the same as the spin of the upper surface of IrMn, thus the magnetization should be uniformly distributed. However, in remanent state B, opposite spin directions at the adjacent atom planes of FM and AFM layers will be an extremely high-energy state; gradual variation of spin orientation such as springlike spin structure extending to the FM layer is energetically more favorable. So, the antiparallel case offers an opportunity to detect the dimension of the springlike spin structure near the CoFeB/IrMn interface.

Figures 6(b) and 6(c) are the phase images caused only by magnetic information corresponding to points A and B in Fig. 6(a), respectively. Figures 6(d) and 6(e) show the gradients of phase profiles along lines $A1$–$A3$ in Fig. 6(b) and $B1$–$B3$ in Fig. 6(c), respectively. The contour lines are uniformly distributed from the upper edge of the CoFeB to CoFeB/IrMn interface in both cases and no distinct difference can be observed from phase images and derivatives of phase profiles. That is, within the spatial resolution of ∼2.3 nm, the remanent state of the high-resolution holography image suggests that the springlike spin structure might vary finitely near the interface. This takes us to the previous works [10–15]; they found an asymmetric magnetization reversal resulting from the FM domain structure near the interface, and that a symmetry breaking at the interface between the two layers mainly affects the results. The key of this problem thus falls onto the size of the symmetry-breaking region. From our direct-imaging results, this region, if it exists, must be subnanometer near the interface. Recently, through producing an ideal interface, a huge H_{EB} has been achieved in the magnetic phase separation system [31,32].

IV. SUMMARY

In situ observation of magnetic switching in CoFeB/IrMn exchange-bias system was demonstrated firstly. The transition of magnetic switching process is abrupt and no intermediated magnetic state is detected with 10-Oe magnetic-field step, implying that there is no springlike domain wall in a wide range of the FM layer. Within the spatial resolution of ∼2.3 nm, the uniform remanent state of the high-resolution holography image suggests that the region of springlike spin structure, if it exists, must be subnanometer. Thus, the model of exchange coupling in inhomogeneous magnetic systems should be considered carefully from the theoretical part to design new structure with a large H_{EB} and large coercivity, which is also important for designing both exchange-bias systems and rare-earth-free permanent magnets comprising two magnetic phases.

ACKNOWLEDGMENTS

We would like to thank Prof. Yimei Zhu and Prof. Junling Wang for fruitful discussions, and Mr. Chiming Jin and Prof. Haifeng Du for the preparation of TEM samples. This work was supported by National Key R&D Program of China (Grants No. 2016YFA0201102 and No. 2016YFA0300103), the National Natural Science Foundation of China (Grants No. 51571208, No. 51301191, No. 51525103, No. 51790491, No. 11474295, and No. 51332007), the Youth Innovation Promotion Association of the Chinese Academy of Sciences (Grant No. 2016270), Overseas, Hong Kong & Macao Scholars Collaborated Researching Fund (Grant No. 51428201), the Key Research Program of the Chinese Academy of Sciences (Grant No. KJZD-EW-M05), the Instrument Developing Project of the Chinese Academy of Sciences (Grant No. YZ201536), Ningbo Major Project for Science and Technology (Grant No. 2014B11011), and Ningbo Science and Technology Innovation Team (Grant No. 2015B11001).

S.H. and K.P. contributed equally to this work.

[1] W. H. Meiklejohn and C. P. Bean, Phys. Rev. **102**, 1413 (1956).

[2] J. Nogués, J. Sort, V. Langlais, V. Skumryev, S. Suriñach, J. S. Muñoz, and M. D. Baró, Phys. Rep. **422**, 65 (2005).

[3] S. Gider, B. U. Runge, A. C. Marley, and S. S. P. Parkin, Science **281**, 797 (1998).
[4] V. Skumryev, S. Stoyanov, Y. Zhang, G. Hadjipanayis, D. Givord, and J. Nogues, Nature (London) **423**, 850 (2003).
[5] S. M. Wu, S. A. Cybart, P. Yu, M. D. Rossell, J. X. Zhang, R. Ramesh, and R. C. Dynes, Nat. Mater. **9**, 756 (2010).
[6] E. Lage, C. Kirchhof, V. Hrkac, L. Kienle, R. Jahns, R. Knoechel, E. Quandt, and D. Meyners, Nat. Mater. **11**, 523 (2012).
[7] W. H. Meiklejohn, J. Appl. Phys. **33**, 1328 (1962).
[8] R. Morales, Z.-P. Li, J. Olamit, K. Liu, J. M. Alameda, and I. K. Schuller, Phys. Rev. Lett. **102**, 097201 (2009).
[9] M. Y. Khan, C.-B. Wu, and W. Kuch, Phys. Rev. B **89**, 094427 (2014).
[10] R. Morales, A. C. Basaran, J. E. Villegas, D. Navas, N. Soriano, B. Mora, C. Redondo, X. Batlle, and I. K. Schuller, Phys. Rev. Lett. **114**, 097202 (2015).
[11] P. Miltenyi, M. Gierlings, J. Keller, B. Beschoten, G. Guntherodt, U. Nowak, and K. D. Usadel, Phys. Rev. Lett. **84**, 4224 (2000).
[12] M. R. Fitzsimmons, P. Yashar, C. Leighton, I. K. Schuller, J. Nogues, C. F. Majkrzak, and J. A. Dura, Phys. Rev. Lett. **84**, 3986 (2000).
[13] P. Blomqvist, K. M. Krishnan, and H. Ohldag, Phys. Rev. Lett. **94**, 107203 (2005).
[14] K. Liu, S. M. Baker, M. Tuominen, T. P. Russell, and I. K. Schuller, Phys. Rev. B **63**, 060403(R) (2001).
[15] Z. P. Li, O. Petracic, R. Morales, J. Olamit, X. Batlle, K. Liu, and I. K. Schuller, Phys. Rev. Lett. **96**, 217205 (2006).
[16] W. Zhang, Y. Zhai, M. Lu, B. You, H. Zhai, and G. M. Caroline, Chin. Phys. B **24**, 047502 (2015).
[17] Z. B. Guo, Y. H. Wu, J. J. Qiu, B. Y. Zong, and G. C. Han, Phys. Rev. B **78**, 184413 (2008).
[18] H. S. Park, X. Yu, S. Aizawa, T. Tanigaki, T. Akashi, Y. Takahashi, T. Matsuda, N. Kanazawa, Y. Onose, D. Shindo, A. Tonomura, and Y. Tokura, Nat. Nanotech. **9**, 337 (2014).
[19] A. Masseboeuf, A. Marty, P. Bayle-Guillemaud, C. Gatel, and E. Snoeck, Nano Lett. **9**, 2803 (2009).
[20] L. Marin, L. A. Rodriguez, C. Magen, E. Snoeck, R. Arras, I. Lucas, L. Morellon, P. A. Algarabel, J. M. De Teresa, and M. R. Ibarra, Nano Lett. **15**, 492 (2015).
[21] D. Reyes, N. Biziere, B. Warot-Fonrose, T. Wade, and C. Gatel, Nano Lett. **16**, 1230 (2016).
[22] L. A. Rodriguez, C. Magen, E. Snoeck, C. Gatel, L. Marin, L. Serrano-Ramon, J. L. Prieto, M. Munoz, P. A. Algarabel, L. Morellon, J. M. De Teresa, and M. R. Ibarra, Ultramicroscopy **134**, 144 (2013).
[23] D. S. Zhang, J. M. Shaw, D. J. Smith, and M. R. McCartney, J. Magn. Magn. Mater. **388**, 16 (2015).
[24] Y.-W. Oh, S.-H. C. Baek, Y. M. Kim, H. Y. Lee, K.-D. Lee, C.-G. Yang, E.-S. Park, K.-S. Lee, K.-W. Kim, G. Go, J.-R. Jeong, B.-C. Min, H.-W. Lee, K.-J. Lee, and B.-G. Park, Nat. Nanotech. **11**, 878 (2016).
[25] G.-X. Miao, M. Muenzenberg, and J. S. Moodera, Rep. Prog. Phys. **74**, 036501 (2011).
[26] C. Chappert, A. Fert, and F. N. Van Dau, Nat. Mater. **6**, 813 (2007).
[27] J. Nogues and I. K. Schuller, J. Magn. Magn. Mater. **192**, 203 (1999).
[28] E. Völkl, L. F. Allard, and D. C. Joy, *Introduction to Electron Holography*, Springer Science & Business Media, Vol. 268 (Kluwer/Plenum, New York, 1999).
[29] H. Lichte and M. Lehmann, Rep. Prog. Phys. **71**, 016102 (2008).
[30] A. Tonomura, T. Matsuda, J. Endo, T. Arii, and K. Mihama, Phys. Rev. B **34**, 3397 (1986).
[31] B. M. Wang, Y. Liu, P. Ren, B. Xia, K. B. Ruan, J. B. Yi, J. Ding, X. G. Li, and L. Wang, Phys. Rev. Lett. **106**, 077203 (2011).
[32] A. K. Nayak, M. Nicklas, S. Chadov, P. Khuntia, C. Shekhar, A. Kalache, M. Baenitz, Y. Skourski, V. K. Guduru, A. Puri, U. Zeitler, J. M. D. Coey, and C. Felser, Nat. Mater. **14**, 679 (2015).